Milsch, H., Priegnitz, M., Blöcher, G. (2011): Permeability of gypsum samples dehydrated in air. - Geophysical Research Letters, 38, L18304

DOI: 10.1029/2011GL048797

Permeability of gypsum samples dehydrated in air

Harald Milsch,[1] Mike Priegnitz,[1] and Guido Blöcher[1]

Received 6 July 2011; revised 19 August 2011; accepted 22 August 2011; published 20 September 2011.

[1] We report on changes in rock permeability induced by devolatilization reactions using gypsum as a reference analog material. Cylindrical samples of natural alabaster were dehydrated in air (dry) for up to 800 h at ambient pressure and temperatures between 378 and 423 K. Subsequently, the reaction kinetics, so induced changes in porosity, and the concurrent evolution of sample permeability were constrained. Weighing the heated samples in predefined time intervals yielded the reaction progress where the stoichiometric mass balance indicated an ultimate and complete dehydration to anhydrite regardless of temperature. Porosity showed to continuously increase with reaction progress from approximately 2% to 30%, whilst the initial bulk volume remained unchanged. Within these limits permeability significantly increased with porosity by almost three orders of magnitude from approximately 7×10^{-19} m^2 to 3×10^{-16} m^2. We show that - when mechanical and hydraulic feedbacks can be excluded - permeability, reaction progress, and porosity are related unequivocally. **Citation:** Milsch, H., M. Priegnitz, and G. Blöcher (2011), Permeability of gypsum samples dehydrated in air, *Geophys. Res. Lett.*, *38*, L18304, doi:10.1029/2011GL048797.

1. Introduction

[2] Devolatilization reactions have been suggested to play a key role for fluid transport, fluid budget, and seismicity in metamorphic environments and particularly in subduction zones [e.g., *Kirby et al.*, 1996; *Hacker et al.*, 2003; *Milsch and Scholz*, 2005; *Brantut et al.*, 2011]. Experimentally, three devolatilization reactions received particular emphasis in this context: (R1) the reaction quartz + calcite → wollastonite + CO_2, (R2) the dehydration of serpentinite to olivine + talc + H_2O, and (R3) the dehydration of gypsum as in the present case. Since the seminal studies by *Raleigh and Paterson* [1965] and *Heard and Rubey* [1966] the majority of investigations were focused on mechanical and hydraulic effects associated with such reactions (e.g., grain size sensitive flow, rock embrittlement, excess pore pressures, and fluid expulsion). *Llana-Fúnez et al.* [2007], *Arkwright et al.* [2008], and *Rutter et al.* [2009] provide recent literature reviews on these topics. Only three studies were identified where direct permeability measurements during an ongoing devolatilization reaction were performed (R1 [*Zhang et al.*, 2000]; R2 [*Tenthorey and Cox*, 2003]) or were attempted (R1 [*Milsch et al.*, 2003]). We have no indication of published permeability data for dehydrating gypsum (R3).

[3] Gypsum has repeatedly been used as an analog material principally for its abundance and its low dehydration temperature. *Ballirano and Melis* [2009] concluded that in air, at a water vapor partial pressure of ca. 1.4 kPa, and in the temperature range of 348 to 403 K, gypsum ($CaSO_4 \bullet 2H_2O$) dehydrates to γ-anhydrite ($CaSO_4$) via an intermediate step forming hemihydrate (bassanite; $CaSO_4 \bullet 0.5H_2O$) first:

$$CaSO_4 \bullet 2H_2O \rightarrow CaSO_4 \bullet 0.5H_2O + 3/2\ H_2O \rightarrow CaSO_4 + 2\ H_2O. \quad (1)$$

An interplay between reaction progress and rock permeability becomes evident when one compares the molar volumes [e.g., *Deer et al.*, 1992] of the educt and solid products involved in the transformation of gypsum (74.53 cm^3/mol) to bassanite (53.17 cm^3/mol) and anhydrite (45.68 cm^3/mol), respectively. One notices that, at ambient conditions, the solid volume decreases by approximately 29% and 39% for the complete transformation to bassanite and anhydrite, respectively. Intuitively but depending on pore connectivity, a decrease in solid volume increases the porosity and therefore should yield an increase in permeability to an extent that is ultimately linked to the reaction progress. On the other hand, if the produced fluid can leak from a stressed reactive rock, pore pressure decreases eventually yielding pore collapse by compaction and consequently a decrease in permeability. In this case all reaction induced effects will be transient. In terms of a reference study we chose an experimental strategy that eliminates both mechanical and hydraulic feedbacks. In addition to permeability, we report on the reaction kinetics and the porosity evolution of the samples and finally derive the interrelations between these parameters.

2. Sample Material and Experimental Procedures

2.1. Sample Material

[4] A slab $30 \times 30 \times 10$ cm^3 of natural quarried alabaster gypsum was purchased from Alabastri Vanzi, Volterra, Italy. This type of material was also used in previous rock physical studies on gypsum (S. Llana-Fúnez, personal communication, 2010). The material appears homogeneous, dense and contains no visible flaws or fractures. Cores of 25 mm in diameter were drilled from this block and the end faces were surface-ground yielding a sample length of 50 mm. The dimensions of each sample and its mass (m_0) were measured with a caliper and a Sartorius analytical balance with 10^{-3} g resolution, respectively. Mass measurements were found to be reproducible by $\pm 5 \times 10^{-3}$ g. The average starting mass of the samples was $m_{0,av} = 55.9 \pm 0.2$ g. Table 1 shows a summary of all samples tested including reaction temperature and time as well as the types of subsequent measurements, if applicable.

2.2. Sample Dehydration

[5] Dehydration of the samples had a twofold purpose: (A) to investigate the transformation kinetics and (B) to later perform porosity and permeability measurements on samples

[1]Deutsches GeoForschungsZentrum GFZ, Potsdam, Germany.

0094-8276/11/2011GL048797

Table 1. Summary of Samples, Measurements and Results

Sample	Temperature (K)	Heating Time (h)	Maximum Transformed Fraction (1)	Kinetics	Porosity (%)	Permeability (10^{-18} m^2)
9_1	293	0	0	—	2.6	—
10_1	293	0	0	—	1.9	—
15	293	0	0	—	2.3[a]	0.7
22	378	800	1.28	x	29.9	281
18	388	27	0.54	—	18.4	182
26	388	39	0.96	—	25.5	253
17	388	185	1.29	x	—	—
16	398	2	0.10	—	4.9[b]	12
10_2	398	4	0.20	—	9.1	50
8	398	7	0.31	—	11.4	70
9_2	398	10	0.44	—	15.1	107
7	398	16	0.81	—	23.0	251
25	398	43	1.14	x	—	—
28	398	67	1.22	x	—	—
12	398	70	1.29	x	—	280
11	398	76	1.27	x	—	—
24	423	42	1.31	—	28.2	249
29[c]	423	48	1.31	—	—	—
23	423	102	1.31	x	28.4	442

[a]Average of samples 9_1 and 10_1.
[b]Calculated with equation (3).
[c]Used only for microstructural investigations and Hg-porosimetry.

reflecting different levels of reaction progress. Four dehydration temperatures, $T = 378$, 388, 398, and 423 K, were selected that should cover both the bassanite and the γ-anhydrite stability field as reported by *Ballirano and Melis* [2009].

[6] Dehydration was performed by heating the samples at a given temperature level for certain time periods in a preheated Memmert UNB400 universal oven with natural air circulation (convection). After heating, the samples were weighed again (m_t) and were then stored in sealed plastic bags and at room temperature to minimize the risk of hydration by air humidity. Subsequent weight measurements proved the appropriateness of this procedure. The mass difference ($m_0 - m_t$) then was the basic quantity to evaluate the reaction progress as outlined in Section 3.2.

2.3. Porosity Measurements and Microstructural Investigations

[7] From the various methods to determine porosity [e.g., *Guéguen and Palciauskas*, 1994] gas-pycnometry was found to be the most appropriate for the present study as it is fast, non-destructive, and inert. Porosity measurements were therefore performed with a Micromeritics AccuPyc helium (He) pycnometer at the Technical University Berlin. A vacuum effect on dehydration was controlled by weighing the samples before and after each measurement and was not observed. Porosity was measured only for selected samples that were further used for permeability measurements (Table 1).

[8] One end member sample was also investigated microstructurally. We selected one sample completely dehydrated to anhydrite at 423 K for 48 h (Table 1). This specimen was saw-cut dry along the vertical axis into two equal halves. One of these halves was used for thin section preparation under water-absent conditions. The thin section was finally investigated optically and with a Scanning Electron Microscope (SEM; Carl Zeiss Ultra 55 Plus) in Secondary Electron (SE) mode. Three SEM-micrographs can be found in the auxiliary material as Figures S1a–S1c.[1] The second half was used for mercury (Hg) porosimetry (Fisons Instruments Porosimeter 2000 WS). The injection curve is shown in the auxiliary material as Figure S2 and will be discussed in Section 3.3.

2.4. Permeability Measurements

[9] Permeability was measured with a conventional gas-permeameter. The use of an inert gas allowed permeability measurements at laboratory temperature conditions (293 ± 1 K) without hydrating a sample and thus destroying the frozen-in microstructure. The permeameter consists of a small pressure vessel, a core holder, pressure gages for confining, up-, and downstream pressure, and three flow meters (MKS Instruments) with a maximum rating of 10, 100, and 1000 ml/min, respectively. The latter were selected depending on sample permeability and related resolution requirements. An impermeable and soft Neoprene sleeve with 25 mm inner diameter was used as the jacket material.

[10] Argon provided from a 20 MPa gas bottle was used as both confining and pore pressure medium. Confining pressure was applied first and one single pressure level of 3 MPa was chosen for all measurements. This level was a compromise between minimizing the risk of instantaneous or transient sample compaction and the flexibility to apply several differential pore pressure steps. Subsequently, pore pressure was applied and flow was initiated with a regulator valve. At steady-state, flow rate was measured at four upstream pressure levels of 0.5, 1, 1.5, and 2 MPa, respectively. The downstream side of the sample was vented to the atmosphere after the flow meters. Finally, permeability was calculated and the Klinkenberg-correction was per-

[1]Auxiliary materials are available in the HTML. doi:10.1029/2011GL048797.

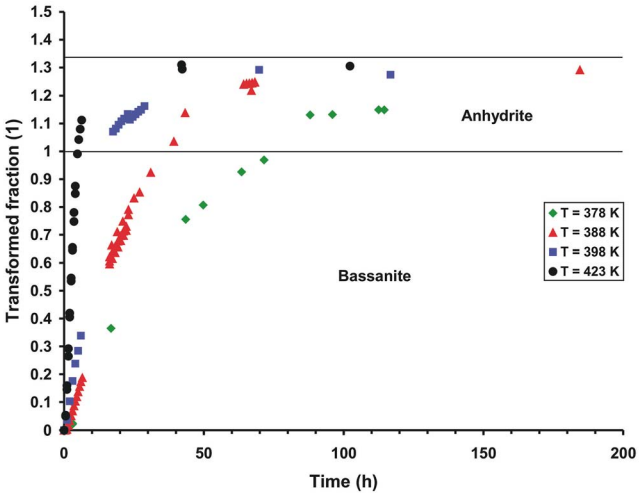

Figure 1. Reaction progress as a function of time. Calculation was based on equation (2) and measured mass differences ($m_0 - m_t$) (Section 3.2). Each point represents an individual mass measurement. One observes an increase in reaction rate with temperature and an ultimate dehydration to anhydrite (α_b close to 1.33) even at 378 K. The respective long-term test (800 h) is not shown for readability but yielded a value of $\alpha_b = 1.28$ (Table 1).

formed following the procedure outlined by *Tanikawa and Shimamoto* [2009].

3. Results and Discussion

3.1. Heating Time

[11] Prior to evaluating the reaction kinetics a numerical simulation was performed to estimate the time required to heat the center of the sample to the oven temperature. In the present case the heating time was minimized by preheating the oven so that the initial temperature boundary conditions were set by the oven temperature T_i at the sample surface and $T_0 = 293$ K elsewhere. For numerically simulating the temperature evolution within a sample of radial symmetry, the open source code OpenGeoSys, v. 4.9.11 [*Wang et al.*, 2009; *Watanabe et al.*, 2010] (http://www.ufz.de/index.php?en=18345) was used. OpenGeoSys allows the implementation of the cylindrical sample geometry as well as the bulk (starting porosity and permeability), solid (gypsum density, thermal expansion, heat capacity, and heat conductivity), and fluid properties (air density, viscosity, heat capacity, and heat conductivity) required for the simulation. The results can then be read from a pvd-file or visualized by, e.g., ParaView 3.6.1. The temperature evolution is asymptotic. The simulation was therefore conducted for all target temperatures T_i until the temperature in the center of the sample was $T_i - 1$ K. The longest heating time calculated was for the run at $T_i = 423$ K to reach $T = 422$ K and was found to be 20 min for the sample dimensions used in this study.

3.2. Reaction Kinetics

[12] Following the procedure outlined in Section 2.2 the mass difference measured ($m_0 - m_t$) yields a direct representation of the bulk reaction progress α. *A priori* it is uncertain whether gypsum transforms to only bassanite or anhydrite at a given temperature. A stoichiometric balance was therefore performed with respect to both minerals by relating the molar masses of the respective solid educt and product as well as the starting and final masses of a sample according to:

$$\alpha_{b,a} = \frac{M_g}{M_g - M_{b,a}} \frac{m_0 - m_t}{m_0}, \tag{2}$$

for bassanite and anhydrite, respectively. Here, M_g, M_b, and M_a are the molar masses of gypsum (172.17 g/mol), bassanite (145.14 g/mol), and anhydrite (136.13 g/mol), respectively. In applying equation (2) it is assumed that all water released by dehydration escapes from a sample. For a representation of the reaction progress in Figure 1, equation (2) with bassanite molar mass was used throughout. This allows an obvious distinction between an ultimate dehydration to bassanite ($\alpha_b = 1$) and anhydrite ($\alpha_b = 1.33$), respectively. This also permits an estimate of the amount of impurities in the samples when $\alpha_b = 1$ or 1.33 is not attained and the reaction progress remains constant after a certain time period.

[13] In Figure 1, each point represents an individual mass measurement. Gaps in the curves indicate nighttimes where no measurements were made. One notices that the reaction rate systematically increased with an increase in dehydration temperature. With regard to the maximum heating time reported in Section 3.1 it showed that the maximum reaction progress during the heating stage itself was only 4% for the runs at 423 K. It is evident that for all temperatures α_b exceeds a value of 1. Also, at 388, 398, and 423 K values of α_b close to 1.33 were observed within heating times not exceeding 100 h. Additionally, a single long-term test conducted at 378 K for 800 h indicates that complete dehydration to anhydrite can also be attained at this temperature (Table 1). It can also be noted that the reproducibility of a test in terms of the observed reaction progress was excellent implying that the material selected was homogeneous in composition and properties. Finally, the impurity content of the samples was found to be less than 1% by mass.

[14] The data was further evaluated to derive a temperature dependent rate law for the overall reaction. As anhydrite was the ultimate reaction product for all temperatures, reaction progress α was calculated using equation (2) with anhydrite molar mass. We then applied the Avrami equation in the form $\alpha = 1 - \exp[-(k_a t)^m]$ and subsequently the Arrhenius equation $k_a = A \exp(-E_a/RT)$, with k_a the rate constant, t the time, m the Avrami exponent, A the frequency factor, E_a the apparent activation energy, and R the universal gas constant. For $T = 378$, 388, 398, and 423 K one obtains $k_a = [4.9, 11.2, 19.8, \text{and } 71.8] \times 10^{-6}$ 1/s as well as $m = 1.32$, 1.37, 1.30, and 1.54, respectively, yielding an activation energy of approximately 78 kJ/mol with no obvious change in transformation mechanism. All parameters k_a, m, and E_a differ significantly from the ones reported by *Ballirano and Melis* [2009] despite environmentally comparable conditions. Therefore, powdered specimens as used by these and other authors (see *Ballirano and Melis* [2009] for reviews) evidently transform differently than polycrystalline aggregates. Furthermore, the derived kinetic parameters k_a, m, and E_a do not necessarily disclose the individual, possibly multi-step, reaction mechanism [e.g., *Ball and Norwood*, 1969] implying a future need for more detailed investigations on the rate-controlling factors.

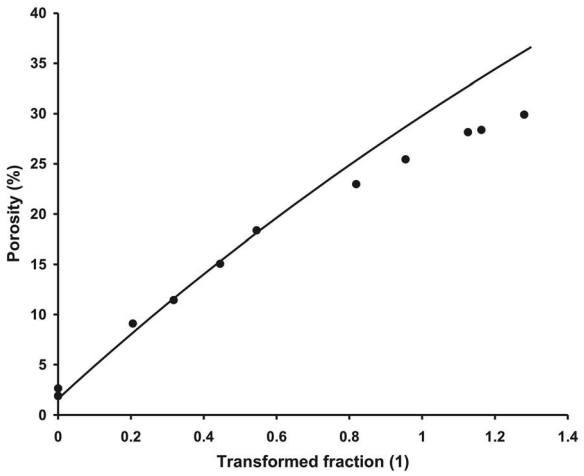

Figure 2. Porosity as a function of reaction progress. Dots represent individual porosity measurements and the calculation of reaction progress α_b was based on equation (2) (Section 3.2). Porosity continuously increased with reaction progress. The line represents the theoretically expected porosity as a function of α_b according to equation (3). One notices a progressive departure of the measured values from the modeled ones for $\alpha_b > 0.6$ (Section 3.3).

3.3. Porosity and Microstructural Evolution

[15] Porosity φ was measured on 11 samples (Table 1) and was observed to continuously increase with reaction progress based on equation (2) (Figure 2, dots). Starting from approximately 2 ± 0.5% at $\alpha_a = \alpha_b = 0$ (pure gypsum) porosity increased to 30% at $\alpha_b = 1.33$ (pure anhydrite), which is about 9% less than theoretically expected for complete dehydration (Section 1).

[16] In Figure 2 the line represents the theoretically expected porosity dependence on reaction progress [$\varphi_b = f(\alpha_b)$] based on the gypsum and bassanite molar mass (equation (2)) and density properties:

$$\varphi_b = 1 - \frac{m_0}{V_0}\left(\frac{1-\alpha_b\left(\frac{M_g - M_b}{M_g}\right)}{(1-\alpha_b)\rho_g + \alpha_b\rho_b}\right), \qquad (3)$$

with V_0, ρ_g, and ρ_b the (initial) sample bulk volume (24.54 cm^3), the gypsum density (2.31 g/cm^3) and the bassanite density (2.73 g/cm^3), respectively. One notices that there is an excellent agreement of the data with the predictions for $\alpha_b < 0.6$. Above, the measured values progressively depart from the modeled ones. In view of the good data quality and the important fact that the bulk volume of the samples did not change this suggests that progressively smaller pores were generated by dehydration. These may not form a percolating cluster and/or pose limitations to the measurement technique itself due to their size, as the typical duration of a single measurement is only ca. 5 min. This finally implies that total porosity was no longer fully determined for $\alpha_b > 0.6$. In fact, when calculating porosity φ_a of end member samples (α_b close to 1.33 in Table 1) via bulk ($\rho_B = m_t/V_0$) and anhydrite densities ($\rho_a = 2.98$ g/cm^3) according to $\varphi_a = 1 - (\rho_B/\rho_a)$ this yields $\varphi_a \approx 39\%$, as expected.

[17] This reasoning is supported by microstructural investigations. Figure S1 shows three SEM-micrographs of a sample completely dehydrated to anhydrite at 423 K for 48 h (Section 2.3 and Table 1) at magnifications of 2 k (a), 15 k (b), and 40 k (c), respectively. One notices a complex microstructure with a larger and connected pore network tracing the initial grain shape of the gypsum crystals (Figure S1a). At higher magnifications, individual former gypsum grains show to be strongly decomposed and a fractal-like microporosity with nm-size channels developed (Figures S1b and S1c). 2D-image analysis performed on Figures S1a and S1c suggests that the dominant porosity accounts for ca. 16% and 23% of the image area, respectively, yielding an excellent agreement with the expected total porosity.

[18] In Figure S2 the Hg-injection curve on the same sample indicates a broad pore radius distribution with nearly all porosity contained within a throat radius interval ranging from 0.02 to 0.5 μm. As for He-pycnometry, theoretical and true total porosity is significantly underestimated, here by ca. 13%. Again, this may indicate a lack in connectivity but might also be due to compaction during injection at high pressure for pore radii <20 nm. However, Hg-porosimetry in the present case was limited to measuring pores >3.8 nm which, in view of Figure S1c, constricts the ability of the technique to account for the total porosity even if it were connected.

3.4. Permeability

[19] Permeability k was measured on 12 samples (Table 1). For each sample and pore pressure step the measurement was performed twice to yield average values and to estimate experimental uncertainties. Measured individual permeability was found to be reproducible within ±20%. Following the procedure described in Section 2.4, Klinkenberg-corrected and average values of permeability are shown in Figure 3 (dots) as a function of measured porosity. At 2% porosity

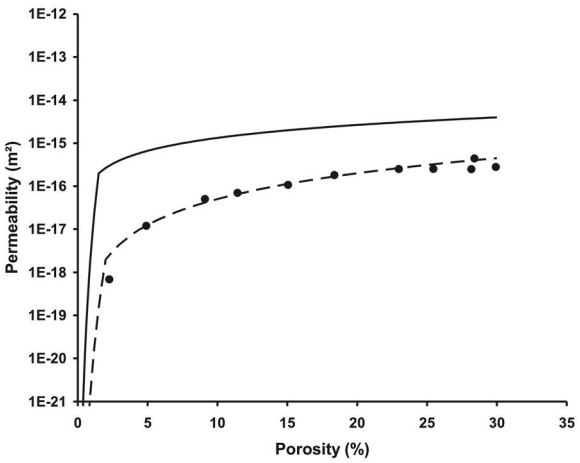

Figure 3. Permeability as a function of measured porosity. Dots represent individual permeability measurements showing a significant increase with reaction progress and thus porosity by three orders of magnitude. The solid line graphically shows the power-law dependence of permeability on porosity proposed by *Wang and Wong* [2003]. One notices that the data departs from this prediction by one to two orders of magnitude, depending on porosity. We found a better representation with a modified power-law (dashed line) according to equation (4) (Section 3.4).

(α_b = 0), permeability was measured as 7×10^{-19} m^2. Permeability then increased dramatically by a factor of 150 to 1×10^{-16} m^2 at 18% porosity (α_b = 0.5). With further reaction progress, permeability only increased slightly to a maximum of $(3 \pm 1) \times 10^{-16}$ m^2 at 30% porosity (α_b = 1.33).

[20] In Figure 3 the solid line represents the two-regime power-law dependence of permeability on porosity proposed by *Wang and Wong* [2003] based on the study by *Ko et al.* [1997] which was conducted wet and at elevated pressures. One notices that the data departs from this prediction by one to two orders of magnitude, depending on porosity. We found a better representation of the data with a modified power-law (dashed line) according to:

$$k = 2 \times 10^{-18} \left(\frac{\varphi}{0.02}\right)^n, \quad (4)$$

with $n = 9$ if $\varphi < 2\%$ and $n = 2$ if $\varphi \geq 2\%$. An exponent $n = 9$ for the percolation regime is somewhat arbitrary due to the lack of data but was chosen for consistency with the study by *Wang and Wong* [2003]. When porosity is fully connected permeability scales with porosity squared corresponding to the tube model suggested by *Gueguen and Dienes* [1989]. An alternative expression of equation (4) can be given within a percolation framework according to $k = f\, 2 \times 10^{-18}\, (\varphi/0.02)^2$, where f is the percolation factor with $f = 1$ if $\varphi \geq 2\%$ and $f = (\varphi/0.02)^7$ if $\varphi < 2\%$. Moreover, equation (4) can be combined with equation (3) to yield an alternative expression relating permeability and reaction progress. When introducing the kinetic results from Section 3.2 into equation (3) one finally obtains rate laws for the temperature dependent evolution of both porosity and permeability.

4. Conclusions

[21] We investigated the effect of dehydration on the permeability evolution of natural gypsum aggregates. Dehydration was performed in air (dry) and, by selecting appropriate experimental procedures and measurement techniques, mechanical and hydraulic feedbacks were excluded. There was no evidence for a particular bassanite stability field as for all temperatures investigated gypsum ultimately dehydrated to anhydrite. The microstructure of the reaction end member (pure anhydrite) was found to be strongly scale dependent including a striking fractal-like microporosity. Total porosity significantly increased to values theoretically predicted, but up to one third may be unconnected. Beyond a percolation regime, permeability scales with the square of porosity implying a tube-like pore network.

[22] In a natural setting (e.g., a subduction zone environment) high permeabilities as observed in this study may provide effective fluid drainage eventually inhibiting embrittlement. However, the devolatilizing rock may transiently compact yielding a shift in the percolation threshold, ultra low permeability despite fluid drainage, and excess pore pressures inducing localized hydraulic fracturing [*Milsch et al.*, 2003]. To what extent these phenomena apply is strongly dependent on the drainage state of the surrounding rock, the external stress conditions, and the intrinsic mechanical properties of the rock matrix and the constituent minerals which in turn also depend on temperature.

[23] Gypsum will continue to be a suitable analog material to study the coupled effects of these parameters on the evolution of a devolatilizing rock system. The results obtained here represent an upper bound reference data baseline for immediate future investigations, e.g., on permeability at elevated pressures and the concurrent microstructural evolution with reaction progress under both dry and wet conditions. This will allow to establish time-dependent physical permeability-porosity relationships but also effective medium bounds, e.g., for P-wave velocity as a second important rock physical parameter.

[24] **Acknowledgments.** We thank Stefan Gehrmann, Helga Kemnitz, Ansgar Schepers, Andreas Kratz, Tobias Meier, and Stephan Strehl for technical assistance. Constructive reviews by Alexandre Schubnel and Nicolas Brantut greatly helped to improve the paper.

[25] The Editor thanks Alexandre Schubnel and Nicolas Brantut for their assistance in evaluating this paper.

References

Arkwright, J. C., E. H. Rutter, K. H. Brodie, and S. Llana-Fúnez (2008), Role of porosity and dehydration reaction on the deformation of hot-pressed serpentinite aggregates, *J. Geol. Soc.*, *165*, 639–649, doi:10.1144/0016-76492007-119.

Ball, M. C., and L. S. Norwood (1969), Studies in the system calcium sulphate-water. Part I. Kinetics of dehydration of calcium sulphate dehydrate, *J. Chem. Soc. A*, *1*, 1633–1637, doi:10.1039/j19690001633.

Ballirano, P., and E. Melis (2009), Thermal behaviour and kinetics of dehydration of gypsum in air from in situ real-time laboratory parallel-beam X-ray powder diffraction, *Phys. Chem. Miner.*, *36*, 391–402, doi:10.1007/s00269-008-0285-8.

Brantut, N., J. Sulem, and A. Schubnel (2011), Effect of dehydration reactions on earthquake nucleation: Stable sliding, slow transients, and unstable slip, *J. Geophys. Res.*, *116*, B05304, doi:10.1029/2010JB007876.

Deer, W. A., R. A. Howie, and J. Zussman (1992), *An Introduction to the Rock-Forming Minerals*, 2nd ed., Prentice Hall, New York.

Gueguen, Y., and J. Dienes (1989), Transport properties of rocks from statistics and percolation, *Math. Geol.*, *21*(1), 1–13, doi:10.1007/BF00897237.

Guéguen, Y., and V. Palciauskas (1994), *Introduction to the Physics of Rocks*, Princeton Univ. Press, Princeton, N. J.

Hacker, B. R., S. M. Peacock, G. A. Abers, and S. D. Holloway (2003), Subduction factory: 2. Are intermediate-depth earthquakes in subducting slabs linked to metamorphic dehydration reactions?, *J. Geophys. Res.*, *108*(B1), 2030, doi:10.1029/2001JB001129.

Heard, H. C., and W. W. Rubey (1966), Tectonic implications of gypsum dehydration, *Geol. Soc. Am. Bull.*, *77*, 741–760, doi:10.1130/0016-7606(1966)77[741:TIOGD]2.0.CO;2.

Kirby, S. H., E. R. Engdahl, and R. Denlinger (1996), Intermediate-depth intraslab earthquakes and arc volcanism as physical expressions of crustal and uppermost mantle metamorphism in subducting slabs, in *Subduction Top to Bottom*, *Geophys. Monogr. Ser.*, vol. 96, edited by G. E. Bebout and D. W. Scholl, pp. 195–214, AGU, Washington, D. C.

Ko, S.-c., D. L. Olgaard, and T.-f. Wong (1997), Generation and maintenance of pore pressure excess in a dehydrating system: 1. Experimental and microstructural observations, *J. Geophys. Res.*, *102*(B1), 825–839, doi:10.1029/96JB02485.

Llana-Fúnez, S., K. H. Brodie, E. H. Rutter, and J. C. Arkwright (2007), Experimental dehydration kinetics of serpentinite using pore volumometry, *J. Metamorph. Geol.*, *25*, 423–438, doi:10.1111/j.1525-1314.2007.00703.x.

Milsch, H. H., and C. H. Scholz (2005), Dehydration-induced weakening and fault slip in gypsum: Implications for the faulting process at intermediate depth in subduction zones, *J. Geophys. Res.*, *110*, B04202, doi:10.1029/2004JB003324.

Milsch, H., W. Heinrich, and G. Dresen (2003), Reaction-induced fluid flow in synthetic quartz-bearing marbles, *Contrib. Mineral. Petrol.*, *146*(3), 286–296, doi:10.1007/s00410-003-0504-8.

Raleigh, C. B., and M. S. Paterson (1965), Experimental deformation of serpentinite and its tectonic implications, *J. Geophys. Res.*, *70*, 3965–3985, doi:10.1029/JZ070i016p03965.

Rutter, E. H., S. Llana-Fúnez, and K. H. Brodie (2009), Dehydration and deformation of intact cylinders of serpentinite, *J. Struct. Geol.*, *31*, 29–43, doi:10.1016/j.jsg.2008.09.008.

Tanikawa, W., and T. Shimamoto (2009), Comparison of Klinkenberg-corrected gas permeability and water permeability in sedimentary rocks, *Int. J. Rock Mech. Min. Sci.*, *46*, 229–238, doi:10.1016/j.ijrmms.2008.03.004.

Tenthorey, E., and S. F. Cox (2003), Reaction-enhanced permeability during serpentinite dehydration, *Geology*, *31*, 921–924, doi:10.1130/G19724.1.

Wang, W. H., and T.-f. Wong (2003), Effects of reaction kinetics and fluid drainage on the development of pore pressure excess in a dehydrating system, *Tectonophysics*, *370*, 227–239, doi:10.1016/S0040-1951(03)00188-4.

Wang, W. Q., G. Kosakowski, and O. Kolditz (2009), A parallel finite element scheme for thermo-hydro-mechanical (THM) coupled problems in porous media, *Comput. Geosci.*, *35*(8), 1631–1641, doi:10.1016/j.cageo.2008.07.007.

Watanabe, N., C. McDermott, W. Wang, T. Taniguchi, and O. Kolditz (2010), Uncertainty analysis of thermo-hydromechanical processes in heterogeneous porous media, *Comput. Mech.*, *45*(4), 263–280, doi:10.1007/s00466-009-0445-9.

Zhang, S., J. D. FitzGerald, and S. F. Cox (2000), Reaction-enhanced permeability during decarbonation of calcite + quartz → wollastonite + carbon dioxide, *Geology*, *28*, 911–914, doi:10.1130/0091-7613(2000)28<911:RPDDOC>2.0.CO;2.

G. Blöcher, H. Milsch, and M. Priegnitz, Deutsches GeoForschungsZentrum GFZ, Telegrafenberg, D-14473 Potsdam, Germany. (milsch@gfz-potsdam.de)